A Robust Visual Servoing Controller for Anthropomorphic Manipulators with Field of View Constraints and Swivel Angle Motion

Jiao Jiang, Yaonan Wang, Yiming Jiang, He Xie, Haoran Tan, Hui Zhang

Abstract—Human-robot collaboration has attracted significant attention in the industry due to the flexibility of humans and the accuracy of robots. Humanoid control of anthropomorphic robotic arms combined with visual servoing will enhance the intelligence of industrial robots. However, the robotic manipulator will introduce psychological discomfort to nearby humans, and the loss of visual features will induce visual servoing task failure. Aiming at these problems, this paper proposes a humanoid control method based on visual servoing by utilizing the swivel angle derived from the human arm to realize the human-like behavior of anthropomorphic robot manipulators. To advance the visual servoing control performance, a constraint function is designed with the Barrier Lyapunov function (BLF) to ensure that image features stay within the field of view. The sliding mode control (SMC) is combined with image-based visual servoing (IBVS) to dispose of the uncertainties of a 7-DOF redundant robot manipulator. The proposed algorithm is substantiated through comparison experiments based on the Sawyer robot and constructed visual servoing physical platform.

I. Introduction

In recent decades, human-like behavior has increased the research interest in various areas such as industrial robots, service robots, and wearable robotic systems. Industrial application is converting from mechanization to anthropomorphism, and in the case of human-robot collaborative work, it can imply a threat to the physical safety of workers. Human-Robot Interaction (HRI) research is a feasible strategy to fix similar problems [1], [2]. Robots with human-like behavior will promote HRI task performance, particularly when industrial robotic manipulators cooperate with workers to accomplish assembly tasks. The human-like motion of an industrial manipulator helps elevate the safety of human-robot cooperation while avoiding discomfort or tension from nearby humans. The upper limb of the human can be modeled as kinematic chains, and the kinematic systems often have human redundancy degrees of freedom [3]. Typical anthropomorphic serial redundant robot manipulators, such as MOTOMAN-SIA (Yaskawa, Fukuoka, Japan) and LBRiiwa (KUKA, Augsburg, Germany), can facilitate HRI task performance because of their human-like behavior and similar mechanical structure to the human arm, which will make robot manipulators more approachable and more socially accepted [4].

This work was supported in part by the National Natural Science Foundation of China under Grants 62293510, 62027810, 62003136 and 62103138; the National Key Research and Development Program of China No. 2021YFB1714700; the Special Funding Support for the Construction of Innovative Provinces of Hunan Province under Grant 2021GK1010; the China Postdoctoral Science Foundation No. BX2021098; Changsha Municipal Natural Science Foundation kq2014060; the Open Research Fund from Guangdong Laboratory of Artificial Intelligence and Digital Economy (SZ), under Grant No. GML-KF-22-14.

Jiao Jiang, Yaonan Wang, Yiming Jiang, He Xie, Haoran Tan, Hui Zhang are with the National Engineering Research Center of RVC, Hunan University, Changsha, China, (email: ymjiang@hnu.edu.cn.)

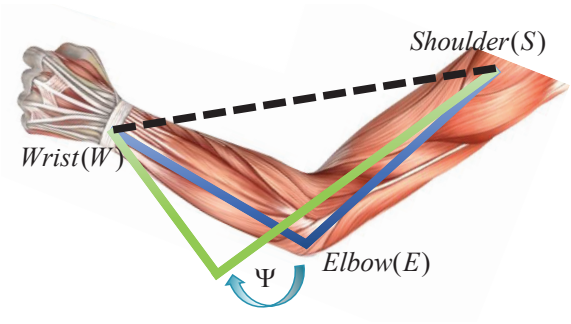

Fig. 1. Definition of the swivel angle of the human arm.

Human-like motions have been implemented on the robot end-effector to improve the task performance of the HRI [5]. A collaborative human-robot manufacturing cell for assembly has been equipped with the end effector of a redundant robot, which can help alleviate the burden on the operator [6]. In [7], remote center of motion (RCM) constraints are employed in combination with an improved recurrent neural network (RNN) for trajectory control of redundant robotic manipulators. However, focusing only on the human-like behavior of the end effector is not enough, since the arm pose will enhance the humanoid control performance.

Employing robot kinematic redundancy can actualize the human-like motion control of redundant robotic manipulators. An elbow elevation angle motion of a human limb is defined to characterize the human arm motions [8]. In [9], to resolve the redundancy of the wearable robotic system, which is similar to the human arm redundancy, they defined the swivel angle Ψ, as shown in Fig. 1. The human-like behavior of the redundant robot manipulator can be introduced by the kinematic model that predicts the relationship between the manipulator and the human arm motion. In [10], incremental learning is employed to optimize the redundancy of an anthropomorphic robot manipulator, and human-like behavior is realized by utilizing swivel motion reconstruction. Deep learning can be considered to realize the humanoid control of the robot manipulator. In [11], deep learning was utilized to develop a human activity recognition system that could perceive

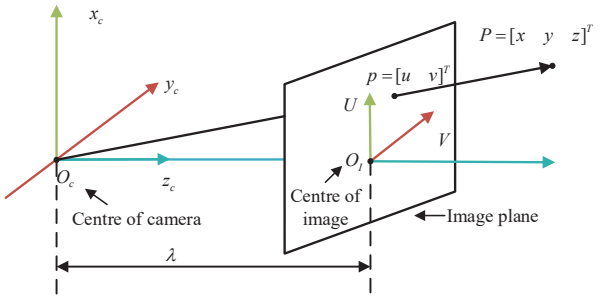

Fig. 2. The geometric model of a pinhole camera.

human dynamic motions.

To make industrial robots behave more like humans, industrial robots are equipped with visual perception functions, which allows robots to complete more complex and flexible work. Visual servoing is widely used in industrial fields to complete tasks such as grasping and assembly. Image-Based Visual Servoing (IBVS) with an eye-in-hand construction is utilized in this paper to reduce the reliance on accurate camera models and avoid the computational burden of pose estimation. Image-based visual servoing improves the efficiency and local stability of vision-guided tasks. Since IBVS only relies on image feature points as a control input, the loss of image features will directly lead to the failure of vision guidance tasks. Therefore, constraining image feature points within the camera's field of view (FOV) is vital to the success of visual servoing tasks.

Numerous research works have been proposed on the problem of image feature loss in visual servoing tasks [12]–[19]. Some research works have attempted to use path planning to avoid image feature trajectories that exceed the camera FOV. In [12], image moment trajectories are designed to solve the image-based control task of the quadrotor, by defining them in the virtual image plane. A trajectory planning algorithm is developed to overcome the shortcomings of visual servoing by parameterizing the velocity screw of the camera and providing an accurate initial depth from the proposed depth estimation technique [14]. Hybrid visual servoing schemes are also employed. In [17], a control framework was designed that combines the advantages of position-based and image-based visual servoing to control a robotic arm-equipped aerial vehicle without losing features during operations. A new wireless hybrid control algorithm is proposed for the visual servoing of mobile robots in [19]. The hybrid algorithm utilizes the position-based visual servoing (PBVS) method for global routing and the IBVS method for fine navigation. The mentioned strategies can guarantee the FOV constraints in the process of visual servoing tasks, but there are many online nonlinear optimization problems, and their real-time feasibility in robotic systems is suspectable.

From the perspective of constraining the image feature output error, the image feature output error does not violate the safety boundary, so it indirectly constrains the image feature points to remain within the preset camera FOV. The Barrier Lyapunov function has been widely used in recent years to constrain the performance of nonlinear systems, and the control law is directly given in the Lyapunov stability analysis process [20]–[23]. In [20], BLF is employed to ensure that a single-input-output nonlinear system stayed within the output constraint. In [21], the properties of BLF are used to constrain the parameters of the unknown function in a compact superset and solve the complex problem of NN approximation conditions. Inspired by these ideas, to address the aforementioned drawbacks and guarantee the success of visual servoing tasks, a BLF is considered in combination with image-based visual servoing to restrain the image feature points that remain within the FOV and guarantee stability of the visual servoing system.

Another problem is the uncertainty of the system dynamics due to the inaccurate modeling of the robotic system, which affects the stability and control accuracy of the visual servo control system. Various solutions have been proposed to this problem, and sliding mode control is a feasible method to improve the robustness of the control system [24]–[27]. In [25], a control method that combines sliding mode control (SMC) and the Takagi-Sugeno fuzzy system model is proposed, which can effectively compensate for the nonlinear disturbance and uncertainty of the robot system. Paper [26] designed a fast integral terminal sliding mode control to handle the system uncertainties of the robotic manipulator. In this research, an SMC control law incorporated with IBVS is advanced to dispose of the uncertainties of 7-DOF redundant robotic manipulators. Motivated by these works, the contributions of this paper are summarized in the following three points:

1) A humanoid algorithm is developed with IBVS control by kinematically reflecting the human-like swivel motion to make the human-robot collaboration capable for most of the typical industrial serial manipulators.
2) The BLF is innovatively introduced to design the controller of the visual servoing system. With the constraint controller, all control variables of the visual servoing system are confined within the bounds of the formed BLF while satisfying FoV constraints.
3) A combined IBVS SMC law is proposed to address the uncertainties of a 7-DoF redundant robot manipulator while elevating the stability of the visual servoing system.

The remainder of the paper is organized as follows. System models and the definition of BLF are given in section *II*. The problem formulation and procedure of the controller design are presented in section *III*. The experimental results are illustrated in *IV*. Finally, the conclusion and discussion are provided in section *V*.

II. Modeling and preliminary

A. System dynamics

The dynamic model of an n-link rigid robot system is usually described as $M(q)\ddot{q} + C(q,\dot{q})\dot{q} + G(q) = \tau$, where $q, \dot{q}$, and $\ddot{q} \in R^n$ are the joint angle position, joint angle velocity and joint angle acceleration variables, respectively. $\tau \in R^n$ are the torque control input variables, $M(q) \in R^{n\times n}$ is the inertia matrix of the robot, $C(q,\dot{q})\dot{q} \in R^n$ is the centripetal and Coriolis force matrix, and $G(q) \in R^n$ is the gravitational matrix. The system dynamics can be described as follows:

$$\frac{d}{dt}\begin{bmatrix} q \\ \dot{q} \end{bmatrix} = \begin{bmatrix} \dot{q} \\ M^{-1}(q)[\tau - C(q,\dot{q})\dot{q} - G(q)] \end{bmatrix}.$$

Define the end-effector velocity as $V_e = [v_e \ \omega_e]^T$, where v_e and ω_e are the translation and rotation velocity, respectively. A mutual conversion between the velocity of the end effector and the joint velocity can be realized by utilizing the Jacobian matrix, and the conversion relationship is $V_e = J_q(q)\dot{q}$, where $J_q(q) \in R^{6\times n}$ is the robot Jacobian matrix, and $\dot{q}$ is the joint velocity of the robot manipulator.

We now consider the visual servoing system with a pinhole camera model mounted at the robot end-effector. A schematic diagram of the projection transformation model of the pinhole camera is shown in Fig. 2. $[x_c \ y_c \ z_c]^T$ represents the axes of the vision system frame C attached at the center of camera O_c. Define a fixed set of 3-D points $P_i = [x_i \ y_i \ z_i]^T, i = 1, ..., m$ in the camera frame; the corresponding 2-D image feature points $s_i = [u_i \ v_i]^T, i = 1, ..., m$ are given as $s_i = \begin{bmatrix} u_i \\ v_i \end{bmatrix} = \frac{\lambda}{z_i}\begin{bmatrix} x_i \\ y_i \end{bmatrix}$, where λ is the focal length of the camera. The relationship between the time variation of the image feature points and the camera velocity V_c can be written as $\dot{s}_i = L_i(z_i, s_i)V_c$, where

$$L_i(z_i, s_i) = \begin{bmatrix} -\frac{\lambda}{z_i} & 0 & \frac{u_i}{z_i} & \frac{u_i v_i}{\lambda} & -\frac{\lambda^2+u_i^2}{\lambda} & v_i \\ 0 & -\frac{\lambda}{z_i} & \frac{v_i}{z_i} & \frac{\lambda^2+v_i^2}{\lambda} & -\frac{u_i v_i}{\lambda} & -u_i \end{bmatrix}$$

is the image interaction matrix; $V_c = [v_c \ w_c]^T$ is the velocity of the camera; v_c and w_c are the linear and angular velocities, respectively.

Define $s = [s_1^T, ..., s_m^T]^T \in R^{2m}$ as the feature point vectors of the whole vision system, and the differential image feature coordinate is obtained

$$\dot{s} = L(z_d, s)V_c$$

where $L(z_d, s) = [L_1^T(z_{d1}, s_1), ..., L_m^T(z_{dm}, s_m)]^T$ is the vision system image interaction matrix, and $z_d = [z_{d1}, ..., z_{dm}]^T$ is the time-varying depth vector. The velocities of the camera V_c and robot end effector V_e can be converted to each other through the formula $V_c = W_{ce}V_e$, where W_{ce} is the screw transformation matrix $W_{ce} = \begin{bmatrix} R_{ce} & [t_{ce}]_\times R_{ce} \\ 0_{3\times 3} & R_{[ce]} \end{bmatrix}$, where $R_{ce} \in SO(3)$ and $t_{ce} \in R^3$ are the rotation matrix and translation vector, respectively. $[t_{ce}]_\times$ is the 3×3 skew-symmetric matrix. In this paper, the W_{ce} is a constant matrix because the camera is rigidly attached to the end-effector. Hence, we can obtain

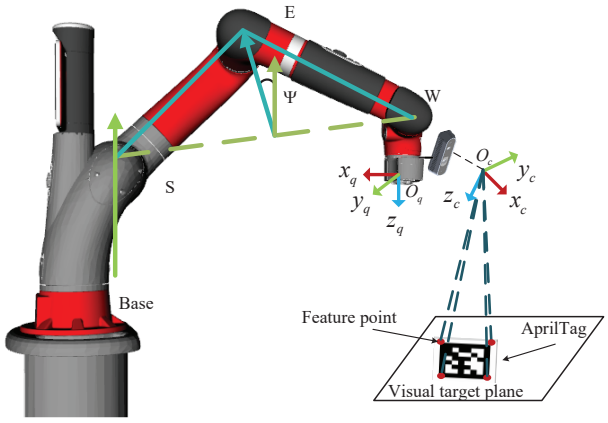

Fig. 3. A schematic diagram of the coordinate transformation relationship and swivel angle defined in the Sawyer robot. S: shoulder; E: elbow; W: wrist.

$$\dot{s} = J_s(z_d, s, q)\dot{q} \tag{1}$$

where $J_s \triangleq LW_{ce}J_q$ is the task Jacobian.

Define $[s^T \ \dot{q}^T]^T \in R^{2m+n}$ as a new state variable of the visual servoing system, combined with the dynamics model of the robotic manipulators, the visual servoing system dynamics can be expressed as:

$$\frac{d}{dt}\begin{bmatrix} s \\ \dot{q} \end{bmatrix} = \begin{bmatrix} J_s(z_d, s, q)\dot{q} \\ M^{-1}(q)[\tau - C(q,\dot{q})\dot{q} - G(q)] \end{bmatrix}.$$

For the convenience of expression, define $x_1 = s, \ x_2 = \dot{q}$, and the system dynamics can be described as

$$\begin{aligned} \dot{x}_1 &= J_s x_2 \\ \dot{x}_2 &= M^{-1}(q)[\tau - C(q,\dot{q})\dot{q} - G(q)] \end{aligned}$$

where $x_1 = [x_{11}, x_{12}, ..., x_{1v}]^T \in R^v, v = 2m$ represent the vector of m image feature points, and x_1 must stay in the set $|x_{1i}| \leq k_{c1i}, i = 1, 2, ..., 2m$. Similarly, the joint velocity vector of the robotic manipulator $x_2 = [x_{21}, x_{22}, ..., x_{2i}]^T, i = 1, 2, ..., n$ is required to satisfy $|x_{2i}| \leq k_{c2i}, , i = 1, 2, ..., n$, where k_{c1} and k_{c2} are set of positive constants.

B. Preliminary

1) Barrier Lyapunov Function (BLF):

Definition 1 [20]: BLF is a scalar function $V(x)$ defined on an open region ξ including the origin relative to the system $\dot{x} = f(x)$, and $V(x)$ is a continuous, positive definite function, which has continuous first-order partial derivatives at each point of ξ. When x approaches the boundary of ξ, $V(x) \to \infty$. For the solution of $\dot{x} = f(x)$ and some positive constant b, $V(x(t)) \leq b, \forall t \geq 0$.

III. Methodology

A. Problem formulation

The visual servoing system consists of an anthropomorphic 7-DOF redundant robotic arm with a depth camera mounted at the end effector, as shown in Fig. 3. O_q is the coordinate origin of tool frame F_q at the geometric center point of the end effector. O_c is the origin of camera frame F_c, which is situated at the projection center of the depth camera. Four points marked in the AprilTag represent four visual feature points. The swivel angle Ψ is defined in the Sawyer robot, which will be described in detail in the following text. The purpose of this research is to propose a visual constraint controller based on IBVS, which is combined with the humanoid control of an anthropomorphic robotic manipulator to make it more intelligent in human-robot collaboration while ensuring the following:

1) The anthropomorphic robotic manipulator can follow a time-varying swivel angle given by the operator and rotate the corresponding angle around the axis formed by the shoulder and the wrist.
2) Image feature points are continuously restricted to the camera FOV without violating the preset safety boundaries.

B. Humanoid-ibvs control

The image-based visual servoing control utilizes the image features to define the control law, and we select points as features. Before proceeding with controller design, we predefine the image feature points tracking error as $z_1 = x_1 - x_d, z_2 = x_2 - \alpha$, where $z_1 = [z_{11}, z_{12}, ..., z_{1v}]^T \in R^v, v = 2m$ are the error signals between the current and the desired feature points; $z_2 = [z_{21}, z_{22}, ..., z_{2n}]^T \in R^n$ correspond to the error signals between the current and the reference joint velocities of the manipulator; and α is the reference velocity, which are designed later.

To simultaneously accomplish the constrained FOV task and humanoid control motion in the redundant robot manipulator, the swivel angle is employed to accomplish human-like control. In Fig. 3, the swivel angle Ψ consists of the angle formed by the actual plane (SEW) and the reference plane (BSW) around the axis $\overrightarrow{SW}$. Ψ can be calculated using geometric relations.

$$\Psi = sgn(\overrightarrow{BS} \times \overrightarrow{SE} \cdot \overrightarrow{SW}) \cdot arccos\left(\frac{(\overrightarrow{BS} \times \overrightarrow{SW})(\overrightarrow{SE} \times \overrightarrow{EW})}{\|\overrightarrow{BS} \times \overrightarrow{SW}\| \|\overrightarrow{SE} \times \overrightarrow{EW}\|} \right) \tag{2}$$

where $\overrightarrow{BS}$ is the vector from the base to the shoulder of the robot, $\overrightarrow{SE}$ is the vector from the shoulder to the elbow of the robot, $\overrightarrow{SW}$ is the vector from the shoulder to the wrist of the robot, and $\overrightarrow{EW}$ is the vector from the elbow to the wrist of the robot. To implement humanoid control, the swivel angle Ψ is projected to null space by utilizing the robot redundancy. The joint velocity in the null space q_N can be calculated by

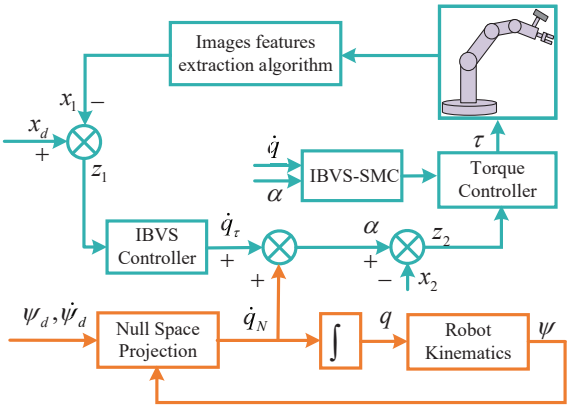

Fig. 4. The control strategy structure of IBVS with humanoid control.

$$\dot{q}_N = J_E^+ \dot{\Psi} \ell_\Psi \tag{3}$$

$J_E \in R^{3\times3}$ is a mapping relationship between the swivel angle Ψ and the null-space joint velocities, which are computed from the robot's elbow to the base. $\dot{\Psi}$ is the differential of Ψ. $\ell_\Psi \in R^{3\times1}$ is defined as the direction vector of the swivel angle motion, expressed as follows:

$$\ell_\Psi = \frac{\overrightarrow{SE} \times \overrightarrow{EW}}{\|\overrightarrow{SE} \times \overrightarrow{EW}\|} \tag{4}$$

To impel the IBVS task constraint's procedure, the BLF is applied to design the IBVS control strategy and choose the Lyapunov function candidateas follows:

$$V_1 = \frac{1}{2} log \frac{k_{a1}^T k_{a1}}{k_{a1}^T k_{a1} - z_1^T z_1} \tag{5}$$

where $k_{a1} = [k_{a11}, k_{a12}, ..., k_{a1i}]^T$, $k_{a1i} = k_{c1i} - A_0$ since $|x_{1i}| < k_{c1i}, i = 1, 2, ..., 2m$ and $\|x_d\| < A_0$, and k_{a1} determines the constraint boundary value. For the visual servoing task, the IBVS position constraint controller $\dot{q}_\tau$ is proposed to track the desired feature point coordinates and restrict them in the camera FOV, which is presented as

$$\dot{q}_\tau = J_s^+ [\dot{x}_d - (k_{a1}^T k_{a1} - z_1^T z_1) k_1 z_1] \tag{6}$$

where $k_1 = [k_{11}, k_{12}, ..., k_{1i}]^T, i = 1, 2, ..., n$ are positive constants, and $\dot{q}_\tau$ represents the required joint velocities that drive the robot to achieve the specified location. In the system dynamics modeling, the image feature coordinates are related to the joint velocities through the task Jacobin matrix.

Differentiating V_1 with respect to time, we can obtain $\dot{z}_1 = J_s(z_2 + \alpha) - \dot{x}_d$. To stabilize the visual servoing system and constrain the visual feature points in the camera FOV,

we design the visual servoing position constraint controller α as follows:

$$\begin{aligned}\alpha =&\dot{q_\tau} + (I - J_q^+ J_q)\dot{q}_N \\ =&J_s^+[\dot{x}_d - (k_{a1}^T k_{a1} - z_1^T z_1)k_1 z_1] \\ &+ (I - J_q^+ J_q)J_E^+ \dot{\Psi}\ell_\Psi \end{aligned} \tag{7}$$

In this work, we assume that the anthropomorphic robotic arm is far away from the singularity, and the pseudo-inverse of the Jacobian matrix exists.

C. Sliding mode torque control

For robot manipulator control, a torque level controller is investigated to actuate the robot to the desired position. The term $M(q)\dot{\alpha}+C(q,\dot{q})\alpha+G(q)$ of the torque controller is unknown, which causes poor control performance. A parameter vector based on the robot manipulator exists to satisfy $M(q)\dot{\alpha}+C(q,\dot{q})\alpha+G(q) = \Phi(q,\dot{q},\alpha,\dot{\alpha})P$, where $\Phi(q,\dot{q},\alpha,\dot{\alpha}) \in R^{n\times l}$ is the regression matrix of known joint variables, and there exists an upper bound $\bar{\Phi}_{ij}$ that satisfies $\bar{\Phi}_{ij} \geq |\Phi_{ij}|, i = 1,...,n, j = 1,...,l$. $P \in R^n$ is an unknown constant parameter vector that describes the mass of the manipulator, and the upper bound $\bar{P_j}$ satisfies $\bar{P_j} \geq |P_j|, j = 1,...,l$. To overcome this problem and improve the control accuracy, $z_2 = \dot{q} - \alpha$ is defined as the sliding surface, and the sliding mode torque controller is designed as follows:

$$\begin{aligned}\tau = &\bar{K}sgn(z_2) - k_2 z_2 - \frac{\dot{x_2} - \dot{\alpha}}{k_{a2}^T k_{a2} - z_2^T z_2} \\ &- (z_2^T)^+ \frac{z_1^T J_s z_2}{k_{a1}^T k_{a1} - z_1^T z_1}\end{aligned} \tag{8}$$

where $\bar{K} = [\bar{K_1}, \bar{K_2}, ..., \bar{K_n}]^T, \bar{K_i} = \sum_{j=1}^{l} \bar{\Phi}_{ij}\bar{P_j}, i = 1,...,n$, and $k_2 = [k_{21}, k_{22}, ..., k_{2i}]^T, i = 1,2,...,n$ are positive constants.

Considering the stability of the visual servoing system, we choose the Lyapunov function candidate V_2 as

$$V_2 = V_1 + \frac{1}{2} log \frac{k_{a2}^T k_{a2}}{k_{a2}^T k_{a2} - z_2^T z_2} + \frac{1}{2} z_2^T M(q) z_2 \tag{9}$$

where $k_{a2} = [k_{a21}, k_{a22}, ..., k_{a2i}]^T$, $k_{a2i} = k_{c2i} - B_0$, since $|x_{2i}| < k_{c2i}, i = 1,2,...,n$ and $\|\alpha\| < B_0$. Parameter k_{a2} determines the constraint boundary of the joint velocity. The control block diagram is presented in Fig. 4.

D. Stability analysis

Theorem 1: Consider the overall dynamic model of the visual servoing control system and the IBVS constraint controller (7) with the constraint torque controller (15) combined with SMC. The initial values of the output error signals z_1 and z_2 are finite, and the initial values of the control input variables $z_1(0)$ and $z_2(0)$ are contained in $\Omega_{z_{10}} := \{z_1 \in R^{2m} : -k_{a1} < z_1 < k_{a1}\}$ and $\Omega_{z_{20}} := \{z_2 \in R^n : -k_{a2} < z_1 < k_{a2}\}$, respectively. The control variables of the visual servoing system will remain in the compact set Ω_{z_1} and Ω_{z_2}, which is defined as follows:

$$\Omega_{z_1} := \{z_1 \in R^{2m} : \|z_{1i}\| \leq k_{a1}\sqrt{(1 - e^{-\xi})}, i = 1,2,...,2m\}$$

$$\Omega_{z_2} := \{z_2 \in R^n : \|z_{2i}\| \leq k_{a2}\sqrt{(1 - e^{-\xi})}, i = 1,2,...,n\}$$

$$\bigcap \{z_2 \in R^n : \|z_{2i}\| \leq \sqrt{\frac{\xi}{\lambda_{min}(M)}}, i = 1,2,...,n\}$$

where $\xi = 2V_2(0)$. The robust FOV constraint control strategy can hold the properties below:

1) The output control variables never violate the preset constraints, i.e., $|x_{1i}| < k_{c1i}, i = 1,2,...,2m, \forall t > 0$;
2) All closed-loop signals are constrained within preset boundaries;
3) The tracking errors z_1 and z_2 of the closed-loop system achieve asymptotic convergence to zero, i.e., $x_1(t) \to x_d(t)$ as $t \to \infty$.

Please see the detailed stability analysis in the appendix.

IV. Experiments

To verify the effectiveness of the proposed humanoid control method based on visual servoing in this paper, a set of comparative experiments is performed. A classical visual servo controller and a PID torque controller are used for control to highlight that our proposed controller with constraints can restrict image features to stay within the camera FOV. The human swivel angle motions are demonstrated during the constraint visual servoing task that aims to validate the feasibility of the proposed humanoid control method. The SMC is utilized for the redundant sawyer robot and aims to improve the stability and accuracy of the humanoid visual servoing control.

A. Experimental setup

To fully verify and study the performance of the FOV constraints approach of humanoid robot control in practice, real-world experiments have been conducted on a physical visual servoing platform that we built. In Fig. 5, we present the overall system. A RealSense D435i camera is equipped on the end-effector of the Sawyer robot, since we adopt the eye-in-hand construction.

The vision section contains the RealSense D435i camera, AprilTag marker, and visual servoing platform (ViSP). ViSP stands for Visual Servo Platform, is a C++ modular, cross-platform library developed by the IRISA-Inria Rainbow team, enables computing control laws and provides a set of visual features for tracking by real-time image processing or computer vision algorithms [28]. The AprilTag image is captured online by the RealSense D435i camera and sent to ViSP. ViSP decodes the tag, extracts the corner coordinates of the AprilTag as feature points, and calculates the visual part control law.

The torque level controller of the Sawyer robot is implemented through Intera SDK, a Python application programming interface developed by the Rethink robotics

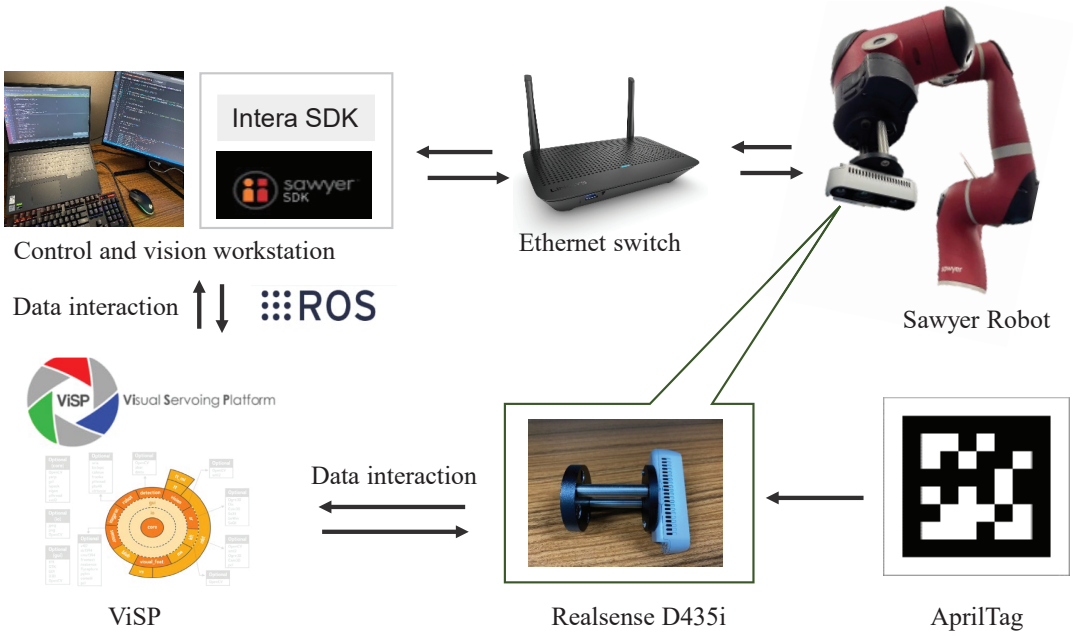

Fig. 5. A physical visual servoing framework. SDK: software development kit.

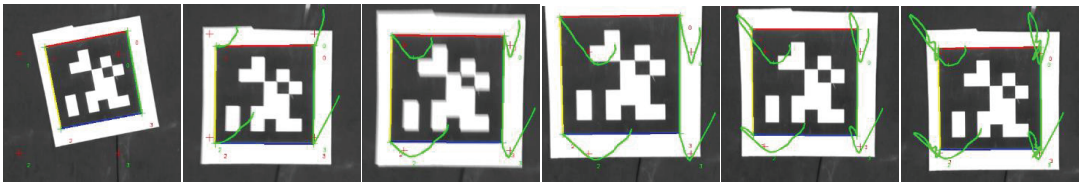

(a)

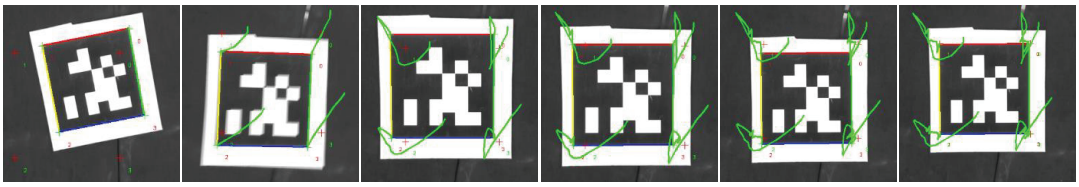

(b)

Fig. 6. A schematic diagram of the actual trajectory of feature points in the camera's FoV (green cross: current feature points; red cross: desired feature points). (a) A classic visual controller and a PID torque controller and (b) a constraint IBVS controller and a sliding mode torque controller. PID: proportional-integral-derivative.

company. The Intera SDK and ViSP are running on a computer equipped with Ubuntu 18.04 and ROS melodic. Because programming languages are not compatible, the ROS topic is utilized to transfer data that interact between two programming platforms.

B. Experimental results

A comparative experiment is presented as follows to verify the proposed algorithm's effectiveness and ensure the stability of the visual servoing system. The controller expression is

$$v_{q1} = -k_1 J_s^T z_1$$
$$\tau_1 = -K_P(e_q(t)) - K_D(z_2(t)) + K_I \int e_q(t)dt$$

where $e_q = q - q_d$, q and q_d are the current joint position and desired joint position, respectively.

For ease of calculation, we map the feature points from the pixel plane to the image plane. Parameter v_{q1} is $k_1 = diag(0.5\ 0.5\ 0.5\ 0.5\ 0.5\ 0.5\ 0.5)$, and parameter τ_1 is $K_P = diag(100\ 80\ 50\ 50\ 36\ 26\ 16), K_I = diag(15.0\ 8.0\ 10.0\ 10.0\ 5.0\ 4.0\ 2.0), K_D =$

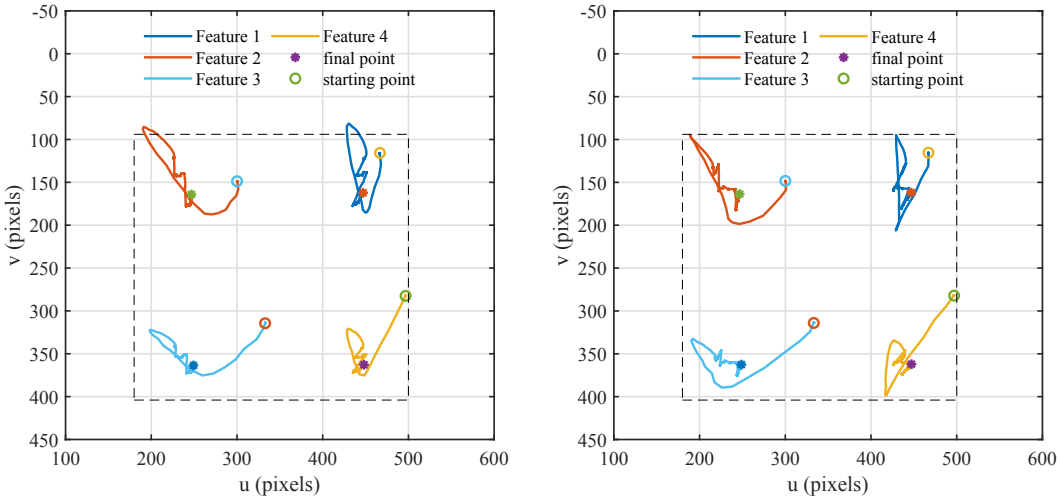

Fig. 7. The trajectory curve of visual features in the pixel plane. (a)A classic visual controller and PID torque controller and (b) a constraint IBVS controller and a sliding mode torque controller. The dotted lines represent the boundary of the camera's FoV, where $u_{max} = 500, v_{max} = 405$ (pixels) and $u_{min} = 180, v_{min} = 95$ (pixels). PID: proportional-integral-derivative.

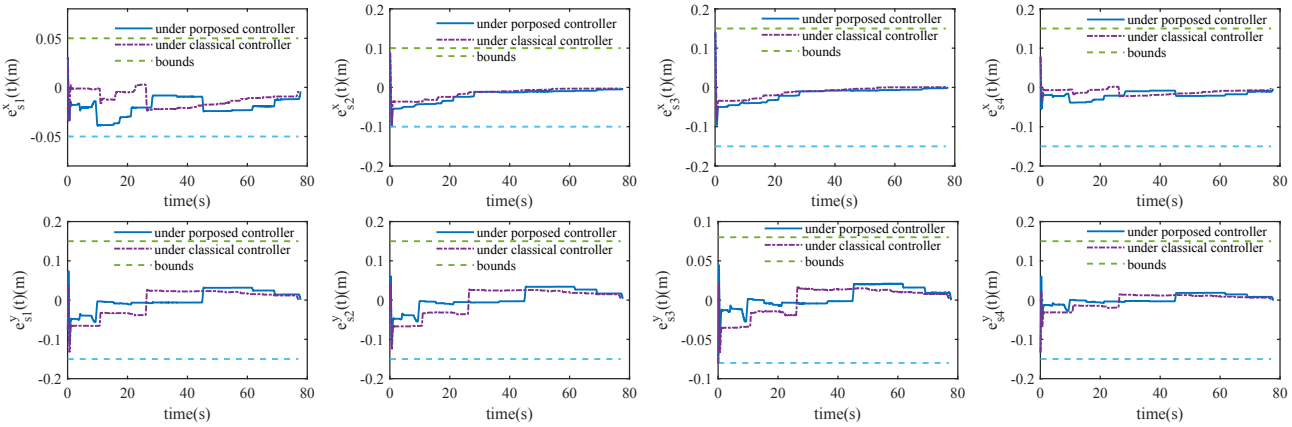

Fig. 8. The convergence curves of all visual feature errors for classical and constrained controllers.

$diag(10.0 \quad 6.0 \quad 5.0 \quad 3.0 \quad 2.6 \quad 1.9 \quad 1.1)$. The parameters of the proposed method are $k_{a1} = [0.05 \quad 0.15 \quad 0.1 \quad 0.15 \quad 0.15 \quad 0.08 \quad 0.15 \quad 0.15]^T$, $k_{a2} = [5 \; 8 \; 5 \; 18 \; 18 \; 18 \; 5]^T$, $\bar{K} = [0.1 \; 0.1 \; 0.1 \; 0.1 \; 0.1 \; 0.1 \; 0.1]^T$, and $k_2 = diag(10.0 \; 6.0 \; 5.0 \; 3.0 \; 2.6 \; 1.9 \; 1.1)$. The initial and desired feature point coordinates are $s_{initial} = [466.5 \; 116.1 \; 300.3 \; 148.9 \; 333.1 \; 314.1 \; 496.4 \; 282.1]^T$ and $s_d = [449.3 \; 161.5 \; 248.2 \; 161.5 \; 248.2 \; 362.6 \; 449.3 \; 362.2]^T$, respectively. The initial and desired joint angles are $q_d = [-0.216 \; -0.704 \; -0.028 \; 1.211 \; 0.034 \; 1.088 \; -0.215]^T$ and $q_{initial} = [-0.0799 \; -0.763 \; -0.184 \; 1.214 \; 0.121 \; 1.164 \; -0.0395]^T$, respectively. The initial joint velocities are $\dot{q} = [0 \; 0 \; 0 \; 0 \; 0 \; 0 \; 0]^T$.

Fig. 6 shows the actual feature point trajectories in the camera view of RealSense D435i. The four corners of AprilTag are selected as image feature points. The red crosses represent the desired image feature point, the green crosses represent the current image feature point, and the green curves are the trajectories of the feature points' movement. To emphasize the performance of the camera FOV constraint algorithm, trajectories of feature points in the pixel plane are presented in Fig. 7. The rectangle box with dotted lines is the camera FOV preset by the operator. Within the hypothetical camera FOV, the trajectories of feature points 1 and 2 are obviously beyond the FOV, as shown in Fig. 7(a). Experiments with our proposed method show that the feature points are successfully constrained in the camera FOV, as shown in Fig. 7(b). Fig.8 shows the convergence curve of the image plane feature point errors. The image feature point position error curves converge in finite time and are

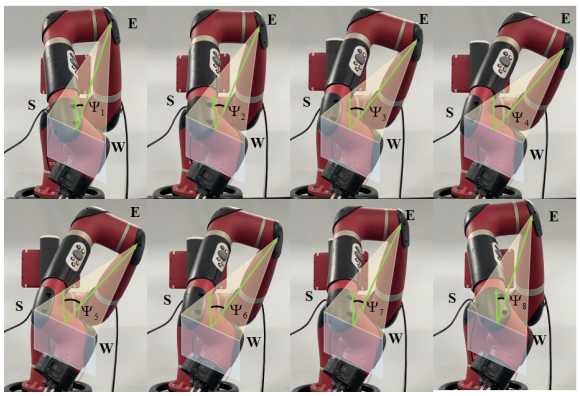

Fig. 9. A humanoid control demonstration of the Sawyer robot. S: shoulder; E: elbow; W: wrist.

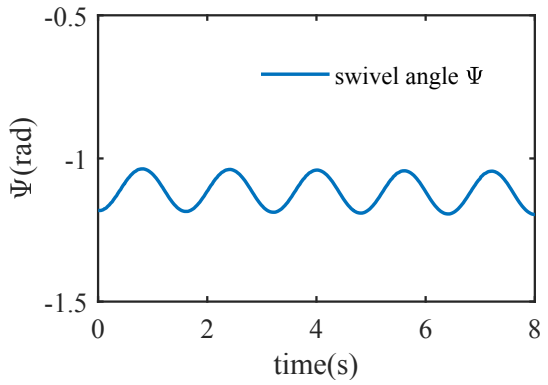

Fig. 10. The curve of swivel angle Ψ.

effectively bounded within the predefined position error bounds. The experimental results confirm the effectiveness of our proposed method.

The human-like motion based on the swivel angle is verified in the Sawyer robot, as shown in Fig. 9. To clarify the validity of the inverse kinematics solution with null-space mapping, the input of the swivel angle is simply set as $\Psi(t) = sin(\pi/4 \times t) * \Psi$. Fig. 10 shows the curve of Ψ, and the redundant robot arm can periodically swing around the axis formed by the shoulder and the wrist according to a set angle and does not interfere with the execution of the end-effector task.

V. Discussion and conclusions

In this paper, swivel angle motion is introduced to realize the human-like control of the anthropomorphic manipulator. The IBVS motion controller with constraints and the torque controller with constraints are designed in combination with the BLF while ensuring that the visual feature coordinates errors respect the FOV constraints. In addition, a sliding mode law with IBVS is designed to address the uncertainty of the visual servo system and enhance the control performance. The experimental results illustrate that the image features can constantly stay within the camera FOV under the constraints introduced by BLF. Comparative experiments were performed to demonstrate the aforementioned theoretical findings.

Further work in the industrial sector will demand more refined and intelligent manipulations for more flexible and diversified operation tasks. Instead of kinematic control, human-robot impedance control can be utilized to intensify the safety and flexibility of the human-robot interaction. More sensors can be combined with vision, such as force sensors, to improve the intelligence of robot manipulators.

APPENDIX

A. Proof of the system stability

Before proceeding with the proof of stability, some useful technical lemmas and properties must be clarified.

Lemma 1: For bounded initial conditions, if there exists a C^1 continuous and positive definite Lyapunov function $V(x)$ satisfying $\kappa_1(\|x\|) \leq V(x) \leq \kappa_2(\|x\|)$, such that $\dot{V}(x) \leq -\rho V(x) + c$, where $\kappa_1, \kappa_2 : R^n \to R$ are class κ functions, and ρ and c are two positive constants, then the solution $x(t)$ is uniformly bounded.

Property 1: The inertia matrix $M(q)$ is symmetric and positive definite, and $\dot{M}(q) - 2C(q, \dot{q})$ is a skew symmetric matrix with the following property [29]

$$\dot{M}(q) - 2C(q, \dot{q}) = 0$$

Property 2: There is a parameter vector that depends on the manipulator parameters $M(q), C(q, \dot{q}), G(q), F(\dot{q})$ and satisfies the linear relationship

$$M(q)\sigma + C(q, \dot{q})\rho + G(q) + F(\dot{q}) = \Phi(q, \dot{q}, \sigma, \rho)P$$

where $\Phi(q, \dot{q}, \alpha, \dot{\alpha}) \in R^{n \times l}$ is the regression matrix of known joint variables, and $P \in R^n$ is an unknown constant parameter vector that describes the mass of the manipulator.

To prove the stability of the whole system, we choose the Lyapunov candidate function as:

$$V_2 = V_1 + \frac{1}{2} log \frac{k_{a2}^T k_{a2}}{k_{a2}^T k_{a2} - z_2^T z_2} + \frac{1}{2} z_2^T M(q) z_2 \qquad (10)$$

where $k_{a2} = [k_{a21}, k_{a22}, ..., k_{a2i}]^T$, $k_{a2i} = k_{c2i} - B_0$ as $|x_{2i}| < k_{c2i}, i = 1, 2, ..., n$ and $\|\alpha\| < B_0$. The derivative of V_2 is given by is given by

$$\begin{aligned} \dot{V}_2 &= \dot{V}_1 + z_2^T[\tau - C(q, \dot{q})\dot{q} - G(q) - M(q)\dot{\alpha}] \\ &\quad + \frac{1}{2} z_2^T \dot{M}(q) z_2 + \frac{z_2^T \dot{z}_2}{k_{a2}^T k_{a2} - z_2^T z_2} \\ &= \dot{V}_1 + z_2^T[\tau - C(q, \dot{q})\alpha - G(q) - M(q)\dot{\alpha}] \\ &\quad + \frac{1}{2} z_2^T [\dot{M}(q) - 2C(q, \dot{q})] z_2 + \frac{z_2^T \dot{z}_2}{k_{a2}^T k_{a2} - z_2^T z_2} \end{aligned} \qquad (11)$$

According to property 1, the value of $\frac{1}{2}z_2^T[\dot{M}(q) - 2C(q,\dot{q})]z_2$ is zero, and we can obtain that

$$\dot{V}_2 = z_2^T[\tau - C(q,\dot{q})\alpha - G(q) - M(q)\dot{\alpha}] - k_1\|z_1\|^2 + \frac{z_1^T J_s z_2}{k_{a1}^T k_{a1} - z_1^T z_1} + \frac{z_2^T \dot{z_2}}{k_{a2}^T k_{a2} - z_2^T z_2} \quad (12)$$

According to property 2, there is a parameter vector based on the robot manipulator that satisfies $M(q)\dot{\alpha}+C(q,\dot{q})\alpha+G(q) = \Phi(q,\dot{q},\alpha,\dot{\alpha})P$, where $\Phi(q,\dot{q},\alpha,\dot{\alpha}) \in R^{n\times l}$ is the regression matrix of known joint variables, and there exists an upper bound $\bar{\Phi}_{ij}$ that satisfies $\bar{\Phi}_{ij} \geq |\Phi_{ij}|, i = 1,...,n, j = 1,...,l$. $P \in R^n$ is an unknown constant parameter vector that describes the mass of the manipulator, and the upper bound $\bar{P}_j$ satisfies $\bar{P}_j \geq |P_j|, j = 1,...,l$. We can obtain

$$\dot{V}_2 = z_2^T[\tau - \Phi(q,\dot{q},\alpha,\dot{\alpha})P] - k_1\|z_1\|^2 + \frac{z_1^T J_s z_2}{k_{a1}^T k_{a1} - z_1^T z_1} + \frac{z_2^T \dot{z_2}}{k_{a2}^T k_{a2} - z_2^T z_2} \quad (13)$$

Considering the Moore-Penrose inverse as follows:

$$z_2^T(z_2^T)^+ = \begin{cases} 0, & z_2 = [0,0,...,0]^T \\ 1, & \text{Otherwise} \end{cases}$$

When $z_2 = [0,0,...,0]^T$, we can deduce that

$$\dot{V}_2 = -k_1 z_1^2 \leq 0 \quad (14)$$

Thus, the system is asymptotically stable according to Barbalat lemma [30]. If $z_2 \neq [0,0,...,0]^T$, define $z_2 = \dot{q} - \alpha$ as the sliding mode surface and design the control input τ as follows:

$$\tau = \bar{K}sgn(z_2) - k_2 z_2 - \frac{\dot{x_2} - \dot{\alpha}}{k_{a2}^T k_{a2} - z_2^T z_2} - (z_2^T)^+ \frac{z_1^T J_s z_2}{k_{a1}^T k_{a1} - z_1^T z_1} \quad (15)$$

where $\bar{K} = [\bar{K_1}, \bar{K_2}, ..., \bar{K_n}]^T, \bar{K_i} = \sum_{j=1}^{l} \bar{\Phi}_{ij}\bar{P}_j, i = 1,...,n$, and $k_2 = [k_{21}, k_{22}, ..., k_{2i}]^T, i = 1,2,...,n$ are positive constants. Thus, we can obtain

$$\begin{aligned} \dot{V}_2 &= -k_1\|z_1\|^2 + [\sum_{i=1}^{n} z_{2i}\bar{K_i}sgn(z_{2_i}) - \sum_{i=1}^{n} k_{2i}z_{2i}^2 - \sum_{i=1}^{n}\sum_{j=1}^{l} z_{2i}\Phi_{ij}P_j] \\ &= -k_1\|z_1\|^2 - k_2\|z_2\|^2 + \sum_{i=1}^{n}|z_{2i}|\bar{\Phi}_{ij}\bar{P}_j - \sum_{i=1}^{n}\sum_{j=1}^{l} z_{2i}\Phi_{ij}P_j \end{aligned} \quad (16)$$

Then, we obtain

$$\dot{V}_2 \leq -k_1\|z_1\|^2 - k_2\|z_2\|^2 < 0 \quad (17)$$

We can deduce that the error signal z_1 satisfies the demand $-k_{a1} < z_1 < k_{a1}$ according to Lemma 1, and the signal z_2 also contains $-k_{a2} < z_2 < k_{a2}$.

References

[1] Yiming Jiang, Chenguang Yang, Yaonan Wang, Zhaojie Ju, Yanan Li, and Chun-Yi Su. Multi-hierarchy interaction control of a redundant robot using impedance learning. Mechatronics, 67:102348, 2020.

[2] Yiming Jiang, Yaonan Wang, Zhiqiang Miao, Jing Na, Zhijia Zhao, and Chenguang Yang. Composite-learning-based adaptive neural control for dual-arm robots with relative motion. IEEE Transactions on Neural Networks and Learning Systems, 2020.

[3] Levi Makaio Miller, Hyunchul Kim, and Jacob Rosen. Redundancy and joint limits of a seven degree of freedom upper limb exoskeleton. In 2011 Annual International Conference of the IEEE Engineering in Medicine and Biology Society, pages 8154–8157. IEEE, 2011.

[4] Andrea Maria Zanchettin, Luca Bascetta, and Paolo Rocco. Acceptability of robotic manipulators in shared working environments through human-like redundancy resolution. Applied ergonomics, 44(6):982–989, 2013.

[5] Haohui Huang, Tong Zhang, Chenguang Yang, and CL Philip Chen. Motor learning and generalization using broad learning adaptive neural control. IEEE Transactions on Industrial Electronics, 67(10):8608–8617, 2019.

[6] Andrea Cherubini, Robin Passama, André Crosnier, Antoine Lasnier, and Philippe Fraisse. Collaborative manufacturing with physical human–robot interaction. Robotics and Computer-Integrated Manufacturing, 40:1–13, 2016.

[7] Hang Su, Yingbai Hu, Hamid Reza Karimi, Alois Knoll, Giancarlo Ferrigno, and Elena De Momi. Improved recurrent neural network-based manipulator control with remote center of motion constraints: Experimental results. Neural Networks, 131:291–299, 2020.

[8] Seungsu Kim, ChangHwan Kim, and Jong Hyeon Park. Human-like arm motion generation for humanoid robots using motion capture database. In 2006 IEEE/RSJ International Conference on Intelligent Robots and Systems, pages 3486–3491. IEEE, 2006.

[9] Hyunchul Kim, Levi Makaio Miller, Aimen Al-Refai, Moshe Brand, and Jacob Rosen. Redundancy resolution of a human arm for controlling a seven dof wearable robotic system. In 2011 Annual International Conference of the IEEE Engineering in Medicine and Biology Society, pages 3471–3474. IEEE, 2011.

[10] Hang Su, Wen Qi, Yingbai Hu, Hamid Reza Karimi, Giancarlo Ferrigno, and Elena De Momi. An incremental learning framework for human-like redundancy optimization of anthropomorphic manipulators. IEEE Transactions on Industrial Informatics, 18(3):1864–1872, 2020.

[11] Wen Qi, Hang Su, and Andrea Aliverti. A smartphone-based adaptive recognition and real-time monitoring system for human activities. IEEE Transactions on Human-Machine Systems, 50(5):414–423, 2020.

[12] Dongliang Zheng, Hesheng Wang, Weidong Chen, and Yong Wang. Planning and tracking in image space for image-based visual servoing of a quadrotor. IEEE Transactions on Industrial Electronics, 65(4):3376–3385, 2017.

[13] Jiuxiang Dong and Jie Zhang. A new image-based visual servoing method with velocity direction control. Journal of the Franklin Institute, 357(7):3993–4007, 2020.

[14] Mohammad Keshmiri, Wen-Fang Xie, and Ahmad Ghasemi. Visual servoing using an optimized trajectory planning technique for a 4 dofs robotic manipulator. International Journal of Control, Automation and Systems, 15(3):1362–1373, 2017.

[15] Xueping Wang, Min Liu, Dripta S Raychaudhuri, Sujoy Paul, Yaonan Wang, and Amit K Roy-Chowdhury. Learning person re-identification models from videos with weak supervision. IEEE Transactions on Image Processing, 30:3017–3028, 2021.

[16] Yi Tang, Baopu Li, Min Liu, Boyu Chen, Yaonan Wang, and Wanli Ouyang. Autopedestrian: an automatic data augmentation and loss function search scheme for pedestrian detection. IEEE transactions on image processing, 30:8483–8496, 2021.

[17] Vincenzo Lippiello, Jonathan Cacace, Angel Santamaria-Navarro, Juan Andrade-Cetto, Miguel Angel Trujillo, Yamnia Rodríguez Rodríguez Esteves, and Antidio Viguria. Hybrid visual servoing with hierarchical task composition for aerial manipulation. IEEE Robotics and Automation Letters, 1(1):259–266, 2015.

[18] Kai Li, Hesheng Wang, Xinwu Liang, and Yanzi Miao. Visual servoing of flexible-link manipulators by considering vibration suppression without deformation measurements. IEEE Transactions on Cybernetics, 2021.

[19] Gossaye Mekonnen, Sanjeev Kumar, and Pushparaj Mani Pathak. Wireless hybrid visual servoing of omnidirectional wheeled mobile robots. Robotics and Autonomous Systems, 75:450–462, 2016.

[20] Keng Peng Tee, Shuzhi Sam Ge, and Eng Hock Tay. Barrier lyapunov functions for the control of output-constrained nonlinear systems. Automatica, 45(4):918–927, 2009.

[21] Beibei Ren, Shuzhi Sam Ge, Keng Peng Tee, and Tong Heng Lee. Adaptive neural control for output feedback nonlinear systems using a barrier lyapunov function. IEEE Transactions on Neural Networks, 21(8):1339–1345, 2010.

[22] Haohui Huang, Chenguang Yang, and CL Philip Chen. Optimal robot–environment interaction under broad fuzzy neural adaptive control. IEEE Transactions on Cybernetics, 51(7):3824–3835, 2020.

[23] Chenguang Yang, Dianye Huang, Wei He, and Long Cheng. Neural control of robot manipulators with trajectory tracking constraints and input saturation. IEEE Transactions on Neural Networks and Learning Systems, 32(9):4231–4242, 2020.

[24] Dianye Huang, Chenguang Yang, Yongping Pan, and Long Cheng. Composite learning enhanced neural control for robot manipulator with output error constraints. IEEE Transactions on Industrial Informatics, 17(1):209–218, 2019.

[25] Yew-Wen Liang, Sheng-Dong Xu, Der-Cherng Liaw, and Cheng-Chang Chen. A study of t–s model-based smc scheme with application to robot control. IEEE Transactions on Industrial Electronics, 55(11):3964–3971, 2008.

[26] Khurram Ali, Safeer Ullah, Adeel Mehmood, Hala Mostafa, Mohamed Marey, and Jamshed Iqbal. Adaptive fit-smc approach for an anthropomorphic manipulator with robust exact differentiator and neural network-based friction compensation. IEEE Access, 2022.

[27] Kunlin Guo, Hang Su, and Chenguang Yang. A small opening workspace control strategy for redundant manipulator based on rcm method. IEEE Transactions on Control Systems Technology, 2022.

[28] E. Marchand, F. Spindler, and F. Chaumette. Visp for visual servoing: a generic software platform with a wide class of robot control skills. IEEE Robotics and Automation Magazine, 12(4):40–52, December 2005.

[29] Tong Heng Lee and Christopher John Harris. Adaptive neural network control of robotic manipulators, volume 19. World Scientific, 1998.

[30] Jean-Jacques E Slotine, Weiping Li, et al. Applied nonlinear control, volume 199. Prentice hall Englewood Cliffs, NJ, 1991.